Pd-Catalyzed C(sp2)–H/C(sp2)–H Coupling of Limonene

Marco Di Matteo, Anna Gagliardi, Alexandre Pradal, Luis F Veiros, Fabrice Gallou, Giovanni Poli

▶ **To cite this version:**

Marco Di Matteo, Anna Gagliardi, Alexandre Pradal, Luis F Veiros, Fabrice Gallou, et al.. Pd-Catalyzed C(sp2)–H/C(sp2)–H Coupling of Limonene. Journal of Organic Chemistry, 2024, 89, pp.10451 - 10461. 10.1021/acs.joc.4c00501 . hal-04679911

HAL Id: hal-04679911

https://hal.sorbonne-universite.fr/hal-04679911v1

Submitted on 28 Aug 2024

HAL is a multi-disciplinary open access archive for the deposit and dissemination of scientific research documents, whether they are published or not. The documents may come from teaching and research institutions in France or abroad, or from public or private research centers.

L'archive ouverte pluridisciplinaire **HAL**, est destinée au dépôt et à la diffusion de documents scientifiques de niveau recherche, publiés ou non, émanant des établissements d'enseignement et de recherche français ou étrangers, des laboratoires publics ou privés.

Distributed under a Creative Commons Attribution 4.0 International License

JOC The Journal of Organic Chemistry

Open Access
This article is licensed under CC-BY 4.0

pubs.acs.org/joc Article

Pd-Catalyzed C(sp^2)−H/C(sp^2)−H Coupling of Limonene

Marco Di Matteo, Anna Gagliardi, Alexandre Pradal,* Luis F. Veiros, Fabrice Gallou, and Giovanni Poli*

Cite This: J. Org. Chem. 2024, 89, 10451−10461 Read Online

ACCESS | Metrics & More | Article Recommendations | Supporting Information

ABSTRACT: Limonene undergoes a regioselective Pd(II)-catalyzed C(sp^2)−H/C(sp^2)−H coupling with acrylic acid esters and amides, α,β-unsaturated ketones, styrenes, and allyl acetate, affording novel 1,3-dienes. DFT computations gave results in accord with the experimental results and allowed for the formulation of a plausible mechanism. The postfunctionalization of one of the coupled products was achieved via a large-scale Sonogashira reaction conducted under micellar catalysis.

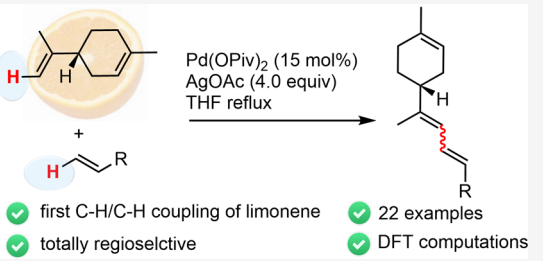

Downloaded via 83.204.172.101 on August 3, 2024 at 11:26:06 (UTC).
See https://pubs.acs.org/sharingguidelines for options on how to legitimately share published articles.

INTRODUCTION

It is widely agreed that the achievement of sustainability with the stop of global warming in our society must pass through the steady decrease of the use of fossil feedstock.[1] On this basis, the gradual replacement of nonrenewable feedstock with biomass appears to be one main measure to take toward this goal.[2] While this transition is already in full swing for the industrial production of alternative fuels, it is not systematically applied in fine chemistry.[3] Accordingly, a major role of today's synthetic chemist consists in valorizing molecules made in bulk amounts by nature, or easily available from waste material, and establishing robust protocols to transform them into drop-in[4] or dedicated[5] biobased molecules[6] of interest in fields such as material and crop sciences, flavor, fragrance, or medicinal chemistry. On the other hand, the catalytic functionalization of an intrinsically unactivated C−H bond in a molecule is a key topic in green chemistry, as it complies with atom- as well as step-economy, adding the C−H bond to the catalogue of the ordinary functional groups, such as halides, alcohols, or carbonyls.[7]

Terpenes are natural hydrocarbons featuring vast structural diversity. Although this class of molecules is considerably less abundant than other primary feedstocks such as lignin, starch, cellulose, proteins, chitin, or triglycerides, they possess a multitude of chemically different C−H bonds.[8] Therefore, their use as starting material for catalytic C−H activation/functionalization processes appears to be an ideal, yet challenging, combination toward sustainability in chemical synthesis. As part of a new, long-term project dedicated to the catalytic C−H/C−H functionalization of terpenes, we decided to first focus our attention on the palladium-catalyzed C−H/C−H cross-coupling of (+)-limonene (Scheme 1).

Available directly as a byproduct of the citrus juice industry or produced biotechnologically by yeasts, limonene is the cheapest monoterpene. With two unsaturations, five allylic C−H bond types (11 C−H bonds in total), and two vinylic C−H bond types (3 C−H bonds in total), it appears a perfect substrate for the development of new C−H activation/functionalization protocols. In this article, we show our results on the Pd-catalyzed regioselective direct C(sp^2)−H/C(sp^2)−H (dehydrogenative) cross-coupling[9−13] between (+)-limonene and alkene partners. To the best of our knowledge, no such cross-coupling has been reported so far, and only two previous C−H functionalizations involving limonene have been described to date. Watson's group[14] reported the Pd-catalyzed C−H borylation of limonene to give the corresponding vinylborane, which could be engaged *in situ* in a Suzuki-Miyaura reaction (Scheme 2, eq 1). A second precedent deals with the Rh-catalyzed hydroformylation of limonene, pioneered by Kollár[15] in 1990, and improved first by Gusevskaya,[16] then by Rieger[17] in 2020 (Scheme 2, eq 2).[18] In a different context, some years ago the group of Loh pioneered nondirected cross-dehydrogenative couplings (CDCs) of intrinsically unactivated 1,1-disubstituted alkenes. In these highly challenging oxidative Pd(II)-catalyzed couplings, alkene reaction partners that are not intrinsically

Scheme 1. General Project: Discovery of Catalytic C−H/C−H Cross-Coupling Reactions Starting from Monoterpenes

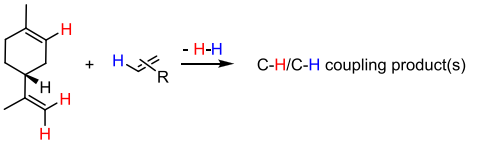

Received: February 25, 2024
Revised: April 12, 2024
Accepted: May 10, 2024
Published: July 18, 2024

© 2024 The Authors. Published by American Chemical Society

Scheme 2. (Top) Precedents of Limonene C−H Functionalization and (Bottom) Precedents of Nondirected Alkene/Alkene CDCs

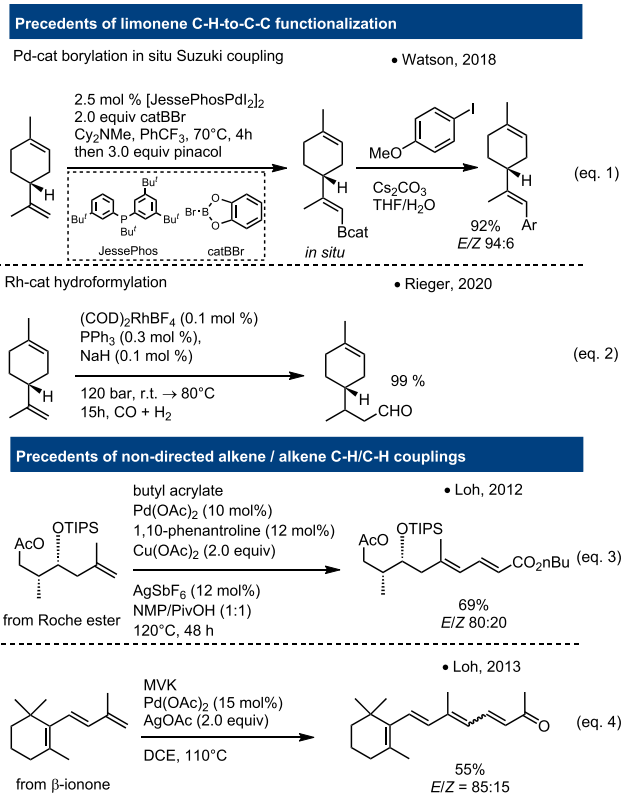

biased for a directed intramolecular metalation come together through C−H bond breaking (Scheme 2, eqs 3 and 4). Thus, building on Loh's results, we undertook the study of undirected Pd-catalyzed C−H/C−H couplings of terpenes, starting with limonene.

RESULTS AND DISCUSSION

Choice of the Model Reaction and Optimization. We started our study by reacting (*R*)-(+)-limonene **1a** and ethyl acrylate **2a**[19] in a 1-to-2 ratio, applying the same reaction conditions as those reported by Loh in 2013. Gratifyingly, under these reaction conditions, a regioselective C9−H/C3−H (limonene numbering) dehydrogenative coupling between the exocyclic alkene of limonene and the *β*-position of the acrylate took place, generating the corresponding sorbate derivative **3aa** in a promising 28% spectroscopic (^{1}H NMR) yield (Table 1, entry 1). The reaction was not stereoselective, generating an almost inseparable *E*/*Z* mixture in a 69:31 ratio. Optimization of the reaction conditions was then undertaken. Among the ethereal solvents (1,4-dioxane, THF, diglyme, and 2-methyltetrahydrofuran), THF turned out to be the best compromise in terms of conversion, yield, and diastereomeric ratio (Table 1, entries 2−5).

Switch to other dipolar aprotic or protic solvents such as DMSO, AcOH, HFIP, DMF, NMP, or a 1:1 v/v mixture of DMSO/PivOH resulted in either low yields or no conversion (Table 1, entries 6−11). The use of $Pd(OCOCF_3)_2$, $PdCl_2(CH_3CN)_2$, PEPPSI-IPr, and $Pd(OPiv)_2$ as palladium sources (Table 1, entries 12−15) in THF gave the final product in 6, 33, 19, and 41% yield, respectively. In summary, $Pd(OAc)_2$ and $Pd(OPiv)_2$ (Table 1, entries 3 and 15) in THF

Table 1. Optimization of the Model C−H-to-C−C Coupling of Limonene[a]

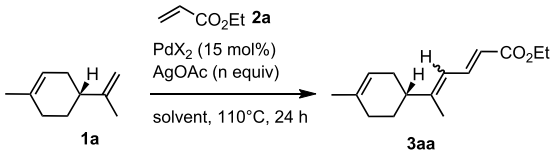

entry	X	*n*	solvent	yield[b]	*E*/*Z*
1	OAc	2.0	DCE	28	69:31
2	OAc	2.0	dioxane	37	67:33
3	OAc	2.0	THF	36	68:32
4	OAc	2.0	diglyme	[c]	
5	OAc	2.0	2-Me-THF	34	66:34
6	OAc	2.0	DMSO	<5	50:50
7	OAc	2.0	AcOH	[c]	
8	OAc	2.0	HFIP	<5	82:18
9	OAc	2.0	DMF	12	51:49
10	OAc	2.0	NMP	9	66:34
11	OAc	2.0	DMSO/PivOH 1:1	5	57:43
12	$OCOCF_3$	2.0	THF	6	64:36
13	$PdCl_2(ACN)_2$	2.0	THF	33	65:35
14	PEPPSI-IPr[d]	2.0	THF	19	62:38
15	OPiv	2.0	THF	41	62:38
16	OPiv	4.0	THF	85	75:25

[a]Reaction conditions: (+)-limonene (0.5 mmol), ethyl acrylate (2.0 equiv), PdX_2 (15 mol %), solvent (0.2 M), and 110 °C in a sealed vial. [b]Measured by quantitative ^{1}H NMR, using 1,4-dinitrobenzene as internal standard. [c]No conversion was observed. [d][1,3-Bis(2,6-Diisopropylphenyl)imidazol-2-ylidene](3-chloropyridyl)palladium-(II) dichloride.

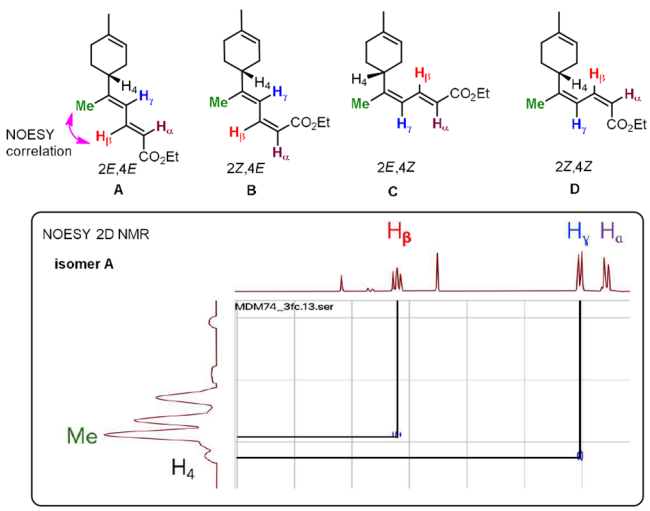

Figure 1. Top: the four possible geometrical isomers of the coupling reaction between **1** and **2**. Bottom: selected region of the NOESY 2D NMR spectrum of major isomer **A**.

turned out to be the best and almost equally performing catalysts. However, due to the variable purity of commercial $Pd(OAc)_2$,[20] we decided to stick to $Pd(OPiv)_2$ for the completion of the study. Finally, keeping the reaction conditions of entry 15 and increasing the amount of AgOAc[21] to 4.0 equiv generated the conjugated dienoate **3aa** in 85% yield and 75:25 4*E*/4*Z* ratio (Table 1, entry 16). Unfortunately, it was not possible to reduce the catalytic

https://doi.org/10.1021/acs.joc.4c00501
J. Org. Chem. 2024, 89, 10451−10461

Scheme 3. Substrate Scope[a]

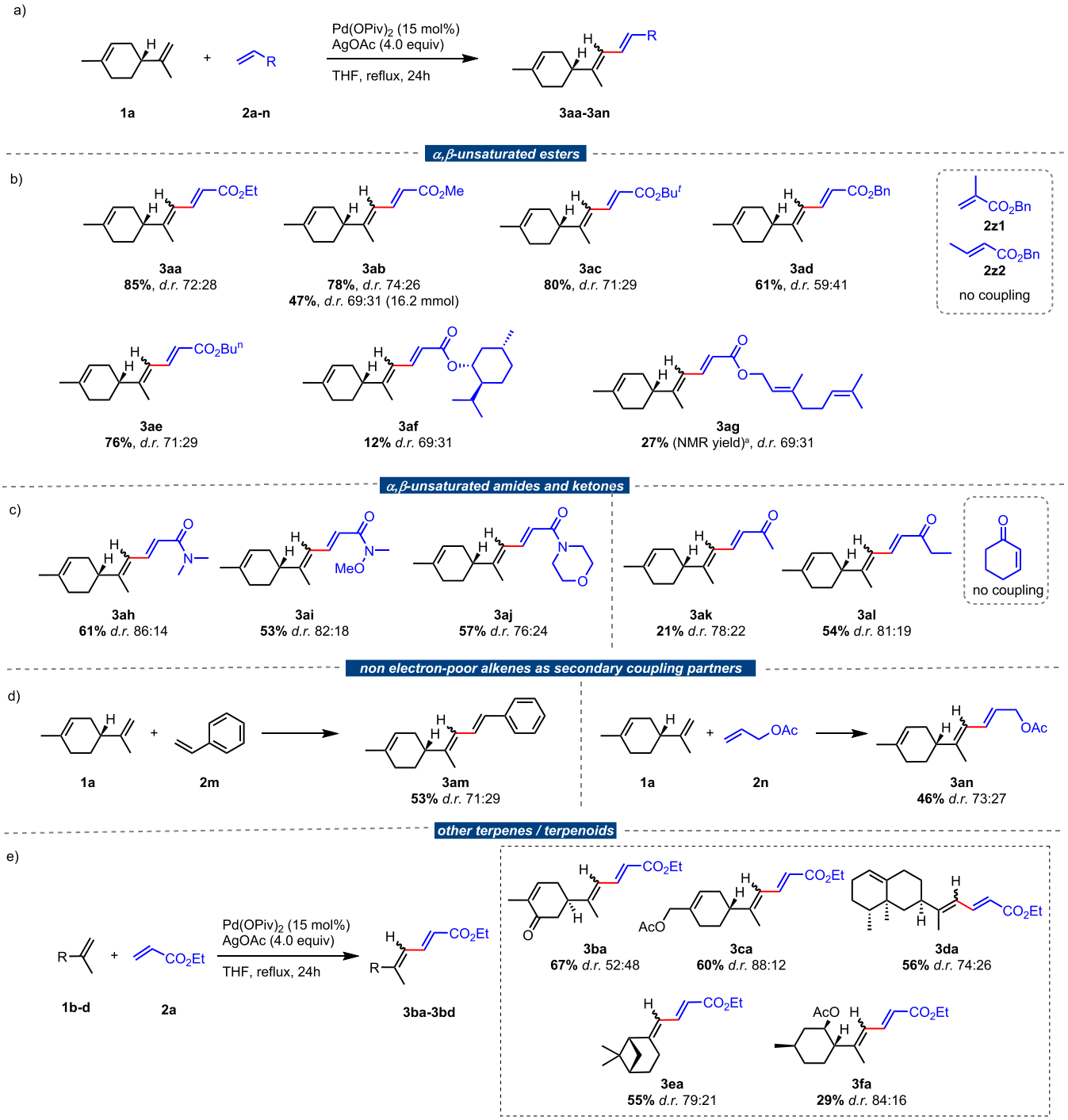

[a]All reactions were performed on 0.5 mmol scale. Unless otherwise stated, percentage represent isolated yields. Reaction conditions: (+)-limonene (0.5 mmol), electron-poor alkene (2.0 equiv), $Pd(OPiv)_2$ (15 mol %), AgOAc (4.0 equiv), THF (0.2 M), and 110 °C (reflux). [b]Yield measured by quantitative ^1H NMR using 1,4-dinitrobenzene as internal standard.

loading of the palladium catalyst[22] nor to switch to greener solvents.[23]

Study of the Selectivity. The coupling generates only two of the four possible geometrical isomers: **A** (2*E*,4*E*), **B** (2*Z*,4*E*), **C** (2*E*,4*Z*), and **D** (2*Z*,4*Z*) (Figure 1, top). Since the vicinal coupling constant $J_{(H\alpha/H\beta)}$ in the ^1H NMR spectrum of the two observed isomers is 11.5 Hz, we can rule out isomers **B** and **D**. Furthermore, a NOESY 2D NMR spectrum of an analytically pure sample of the major isomer showed a correlation between the methyl group on C8 (limonene numbering) and H_β (Figure 1, bottom). This allowed to assign the configuration 2*E*,4*E* to the major isomer **A** and the 2*E*,4*Z* to the minor isomer **C**.

Scope of the C−H/C−H Coupling. After the model reaction was optimized, the scope of this dehydrogenative coupling was evaluated by testing other alkenes as reaction

https://doi.org/10.1021/acs.joc.4c00501
J. Org. Chem. 2024, 89, 10451−10461

Scheme 4. Top: Coupling between (*R*)- or (*S*)-Limonene, and (*S*)-*N*-Methyl-*N*-(1-phenylethyl)acrylamide[a]

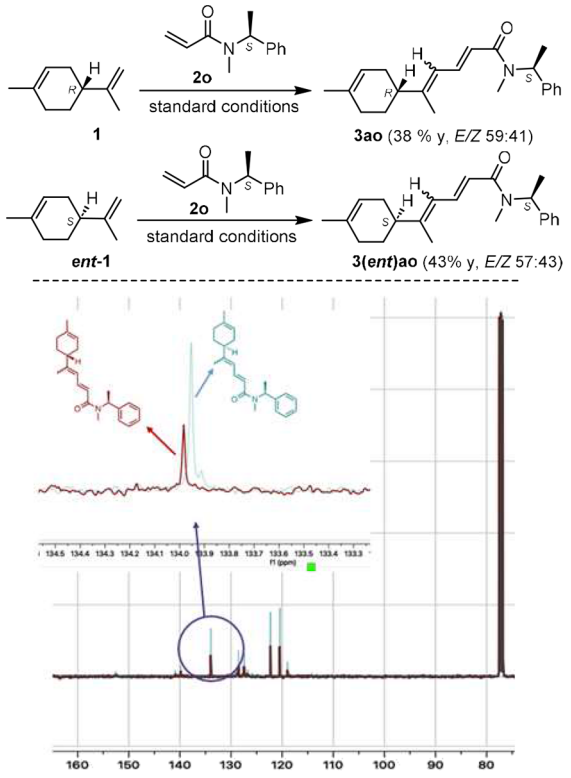

[a]Conditions: $Pd(OPiv)_2$ (15 mol %), AgOAc (4.0 equiv), THF, reflux, 24 h. Bottom: Comparison of the ^{13}C-NMR spectra of the products from the coupling between **1** and **2o**, and between *ent*-**1** and **2o**.

partners for limonene (Scheme 3). Reacting limonene with ethyl, methyl, *t*-butyl, benzyl, and *n*-butyl acrylates under the previously optimized reaction conditions gave the expected corresponding dienoates **3aa**−**3ae** in isolated yields ranging from 61 to 85%.[24] We then considered the influence of substitution of the partner alkene. Unfortunately, no conversion was observed with benzyl methacrylate **2z1**, while only degradation products were generated with benzyl crotonate **2z2**. Thus, the coupling appears to be incompatible with substitutions at the α- and β-positions of the electron-poor alkenes. More complex acrylate esters such as menthyl and geranyl acrylates gave the corresponding coupling products **3af** and **3ag**, although in low yield (Scheme 3, part b).[25]

Tertiary α,β-unsaturated amides were also good coupling partners, giving the expected coupling products **3ah**, **3ai**, and **3aj** in 53−61% isolated yield. These coupling partners appear to be somewhat less efficient, yet, slightly more stereoselective than acrylates.[26] Methyl vinyl ketone and ethyl vinyl ketone reacted too, giving the corresponding conjugated dienes in 21%[27] and 54% isolated yields, respectively. Cyclohex-2-enone gave no conversion, confirming the incompatibility of this protocol with the β-substitution of the α,β-unsaturated alkene (Scheme 3, part c).[28] A couple of non-electron-poor alkenes were also tested as secondary coupling partners. Accordingly, styrene reacted regioselectively at the less substituted alkene position, affording a 71:29 4*E*/4*Z* mixture of the coupled product **3am** in 53% yield, while allyl acetate gave a 73:27 4*E*/4*Z* mixture of the dienyl allylic acetate **3an** in 46% yield (Scheme 3, part d). Keeping ethyl acrylate as the electron-poor coupling partner, the coupling was also tested with other terpenes or terpenoids carrying an isopropenyl moiety besides an endocyclic alkene functional group. Accordingly, carvone, perillyl acetate, valencene, β-pinene, and isopulegol acetate all reacted exclusively at the exocyclic alkene, providing the corresponding coupling products in 67, 60, 56, 55, and 29% yield (Scheme 3, part e).

Check for Potential Racemization/Epimerization. To confirm that the reaction conditions are not affecting the stereogenic allylic center of limonene, we tested and compared the couplings of (*R*)- and (*S*)-limonene with that of (*S*)-*N*-methyl-*N*-(1-phenylethyl)acrylamide **2o**. We reasoned that in the absence of racemization each coupling should afford a couple of enantiopure *EE*/*EZ* products **3ao** and **3**(*ent*)**ao** that are different (diastereoisomeric relation) from each other. Contrarily, the four diastereoisomers (as *E*/*Z* couples) should be produced from each experiment, should the racemization of limonene (or the epimerization of the coupled product) take place. The two couplings were successful, affording products **3ao** and **3**(*ent*)**ao** in 59:41 and 57:43 *E*/*Z* ratio, and 38 and 43% yield, respectively (Scheme 4). A careful comparison of the ^{13}C spectra of the products of the two coupling reactions (each as an *E*/*Z* mixture) showed that they are not fully superimposable. Hence, we confirmed that this coupling does not affect the stereochemical integrity of the allylic stereocenter of limonene.

Study of the Reaction Mechanism. The coupling mechanism between limonene and methyl acrylate to give the sorbate derivative **3ab** was studied via DFT calculations.[29] As four geometrical isomers can in principle be generated, two of which are experimentally observed, we computationally studied all four pathways (the complete profiles are shown in the Supporting Information). The monomeric complex [Pd(II)(bis-κ^2(OAc)$_2$)] **I** was considered as the starting active catalyst (ΔG = 0 kcal/mol as a reference) (Scheme 5, part A). Formation of the aggregate between [Pd(II)(bis-κ^2(OAc)$_2$)] and the exocyclic alkene of limonene is the first step of the catalytic cycle.[30] This endergonic step already biases the geometry of the trisubstituted alkene in the final product. Indeed, the two located complexes $\mathbf{II}_{4E}$ (3.7 kcal/mol, black path) and $\mathbf{II}_{4Z}$ (5.4 kcal/mol, red path) are already en route toward the *E* and *Z* trisubstituted alkenes, respectively. As to the first path, following full π coordination of the exocyclic alkene of limonene to palladium generates intermediate $\mathbf{III}_{4E}$ (ΔG = −4.1 kcal/mol), passing an energetic barrier of 8.8 kcal/mol. In this step, one acetate ligand passes from κ^2 to κ^1-coordination, to allow the π coordination by the alkene. The next step is concerted metalation deprotonation (CMD) wherein the κ^1-bound acetate ligand intramolecularly deprotonates the terminal H atom of exocyclic alkene *trans* to the C_6 ring. The step is endergonic, passing an energetic barrier of 16.0 kcal/mol and generating the σ-vinylpalladium complex $\mathbf{IV}_{4E}$ (2.8 kcal/mol) with the newly generated acetic acid molecule still coordinated. Worthy of note is the metal assistance (d_{Pd-H} = 2.30 Å) in the CMD transition state $\mathbf{TS}_{III4E\rightarrow IV4E}$ (see Figure S1 in the Supporting Information). The step is stereoretentive, in that the palladium atom replaces the position of the deprotonated vinylic H atom. Follows a two-step dissociative, globally exergonic ligand exchange between the exiting acetic acid and the entering acrylate, which generates complex $\mathbf{VII}_{4E}$ (−4.8 kcal/mol, not shown) through a barrier of 15.5 kcal/mol. The subsequent

https://doi.org/10.1021/acs.joc.4c00501
J. Org. Chem. 2024, 89, 10451−10461

Scheme 5. Part A: First Part of the Free Energy Profile of the $Pd(OAc)_2$-Catalyzed/AgOAc-Mediated Coupling between Limonene and Methyl Acrylate; From the Starting Complex to the Carbopalladation Step[a]

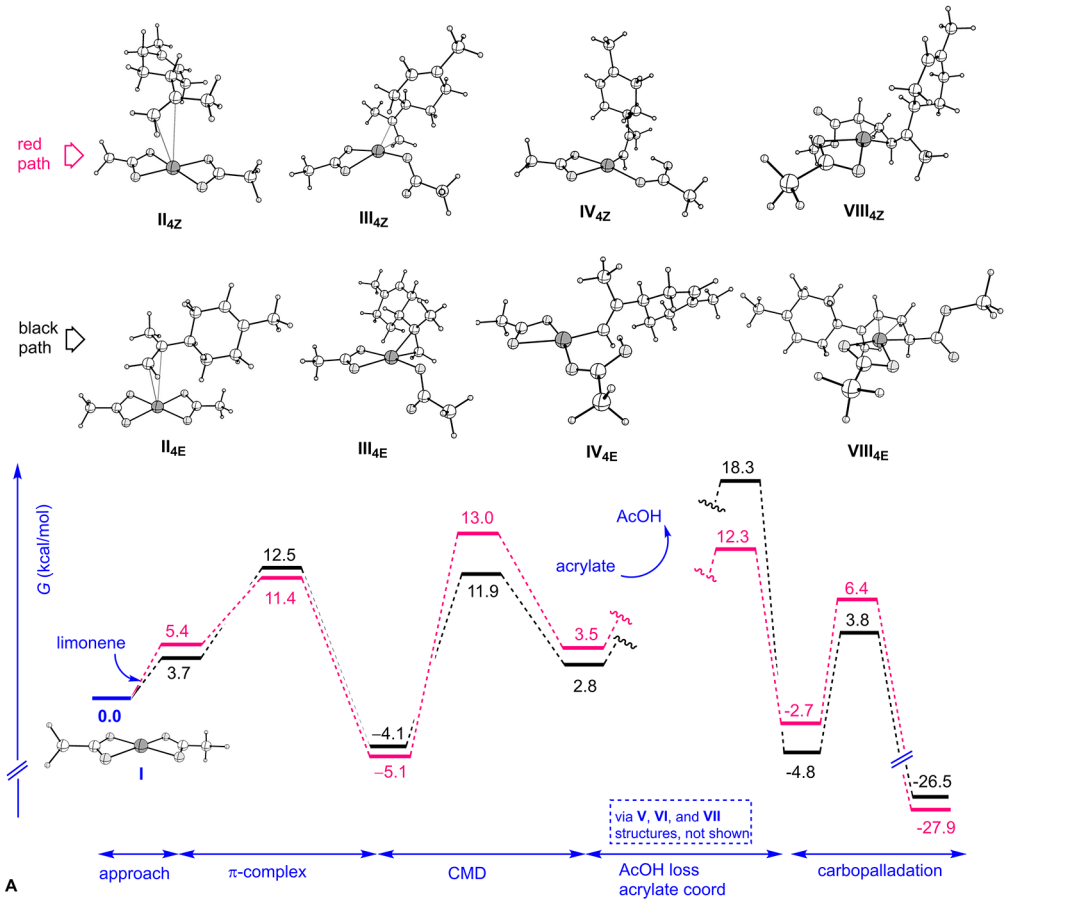

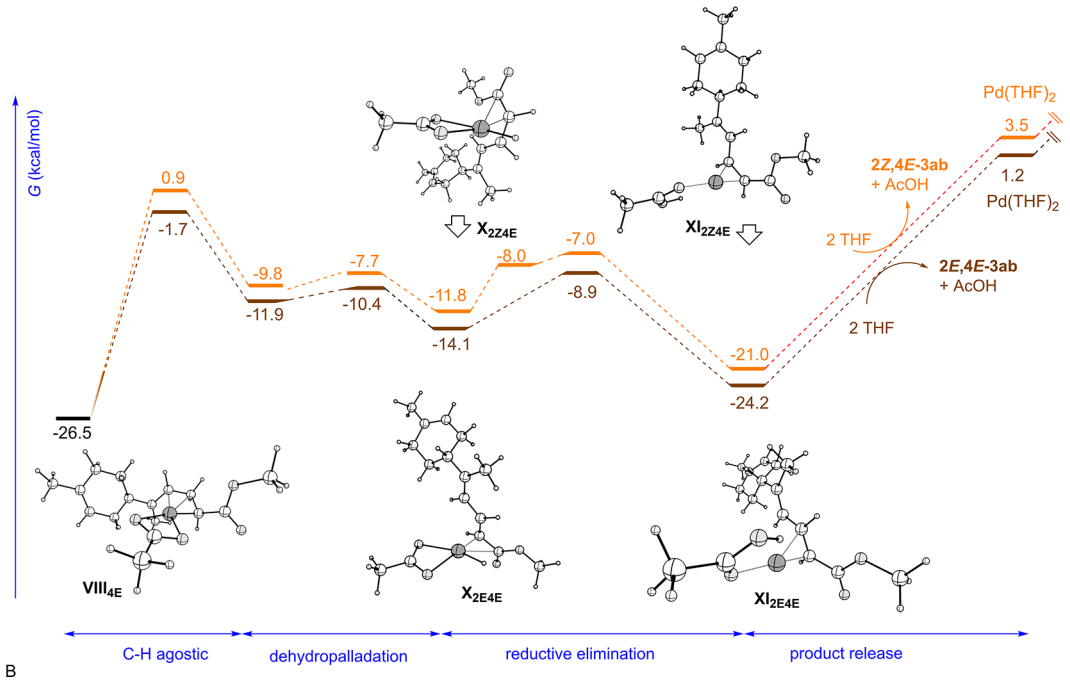

[a]Part B: second part of the energy profile of the $Pd(OAc)_2$ catalyzed/AgOAc-mediated coupling between limonene and methyl acrylate; from the carbopalladation complex **$VIII_{4E}$** to product **2*E*,4*E*-3ab.**

https://doi.org/10.1021/acs.joc.4c00501
J. Org. Chem. 2024, 89, 10451−10461

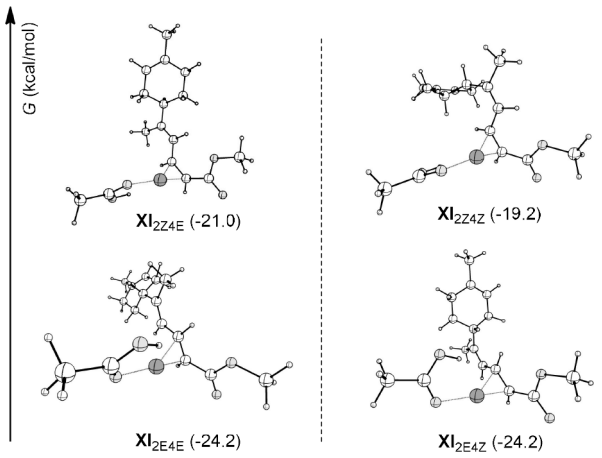

Figure 2. Free energy values of the Pd(0) complexes π-coordinated with the final products and σ-coordinated with acetic acid. Left side: the 4*E* couple (ΔG_{4E} = 3.2 kcal/mol); right side: the 4*Z* couple (ΔG_{4Z} = 5.0 kcal/mol).

Scheme 6. Corollary Experiment to Prove the Reversibility of the Dehydropalladation/Reductive Elimination Sequence

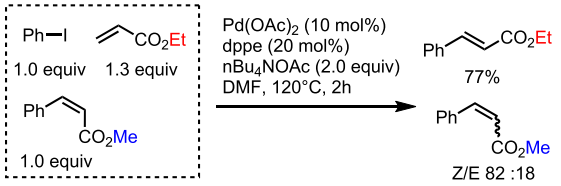

Scheme 7. Final Part of the Free Energy Profile of the $Pd(OAc)_2$-Catalyzed/AgOAc-Mediated Coupling between Limonene and Methyl Acrylate: From Intermediates XI_{2E4E} and XI_{2E4Z} to $Pd(OAc)_2$ Regeneration

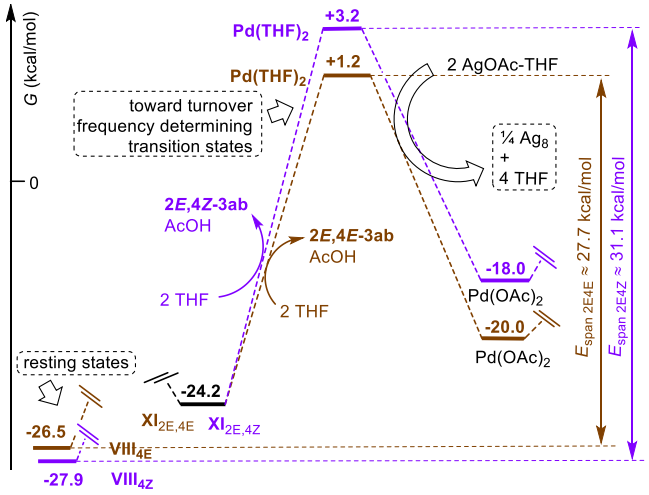

carbopalladation is very exergonic, generating complex $\mathbf{VIII}_{4E}$ (−26.5 kcal/mol), the resting state of the catalytic cycle, via a barrier of 8.6 kcal/mol.

The higher energy aggregate $\mathbf{II}_{4Z}$ follows an analogous [π-complex formation/CMD/AcOH-acrylate ligand exchange/carbopalladation] sequence of steps as the one starting from $\mathbf{II}_{4E}$, leading to intermediate $\mathbf{VIII}_{4Z}$ (−27.9 kcal/mol, red path). The following step for the two paths (black and red) is a dehydropalladation (β-H elimination) (Scheme 5, part B). This globally endergonic two-step transformation lies at the second bifurcation of the mechanism and determines which of the two diastereotopic allylic H atoms at C3 is involved in the agostic interaction, which is in turn associated with the geometry of the 1,2-disubstituted alkene in the product. In one of these two paths (brown path), intermediate $\mathbf{VIII}_{4E}$ generates the hydride complex $\mathbf{X}_{2E4E}$ (−14.1 kcal/mol) stepping over a barrier of 24.8 kcal/mol and passing through the "agostic" intermediate $\mathbf{IX}_{2E4E}$ (−11.9 kcal/mol). The subsequent reductive elimination is exergonic, affording the Pd(0) complex π-coordinated with the final 2*E*,4*E* product and σ-coordinated with acetic acid $\mathbf{XI}_{2E4E}$ (−24.2 kcal/mol), passing a barrier of 5.2 kcal/mol. Then, the final products **2*E*,4*E*-3ab** and acetic acid are released from the complex through the entry into the coordination sphere of two solvent molecules that stabilize the Pd atom. This step is endergonic, reaching +1.2 kcal/mol. The alternative path from intermediate $\mathbf{VIII}_{4E}$ (orange path) follows an analogous [dehydropalladation/reductive elimination/product release] sequence, affording the hydride complex $\mathbf{X}_{2Z4E}$ (−11.8 kcal/mol), passing through the "agostic" intermediate $\mathbf{IX}_{2Z4E}$ (−9.8 kcal/mol), while the subsequent reductive elimination gives $\mathbf{XI}_{2Z4E}$ (−21.0 kcal/mol), and the product release step generates **2*Z*,4*E*-3ab**, $Pd(THF)_2$, and AcOH, rising the energy to +3.5 kcal/mol. Inspection of this second part of the mechanism reveals that the brown path lies consistently at much lower energies than the orange path.

It is important to notice that the barrier for going backward from complexes $\mathbf{XI}_{2E4E}$ and $\mathbf{XI}_{2Z4E}$ to common resting state $\mathbf{VIII}_{4E}$ is lower than the one for going forward toward product release (Scheme 5, part B), and this is also true for the corresponding sequence of steps starting from minor resting state $\mathbf{VIII}_{4Z}$ (see the Supporting Information).

This scenario implies that equilibration between $\mathbf{XI}_{2E4E}$ and $\mathbf{XI}_{2Z4E}$ takes place before product release. Accordingly, the 2*E*/2*Z* ratios in the products are expected to depend on the energy differences between $\mathbf{XI}_{2E4E}$ and $\mathbf{XI}_{2Z4E}$ for the major 4*E* path, and on that between $\mathbf{XI}_{2E4Z}$ and $\mathbf{XI}_{2Z4Z}$ for the minor 4*Z* path. The computed ΔGs highly favor the 2*E* stereochemistry in both cases (ΔG_{4E} = 3.2 kcal/mol; ΔG_{4Z} = 5.0 kcal/mol), which agrees with the fact that only the 2*E* geometrical isomers are experimentally observed (Figure 2).

According to the above results, the catalytic cycle is experimentally viable only for the two paths that at the second branching lead to the 2*E* configurated products. To further support the above-mentioned equilibration between the intermediates $\mathbf{XI}_{2E}$ and $\mathbf{XI}_{2Z}$, a classical Mizoroki-Heck coupling between ethyl acrylate and phenyl iodide was carried out [$Pd(OAc)_2$ (10 mol %), dppe (20 mol %), nBu$_4$NOAc (2.0 equiv), DMF, 120 °C, 2 h] in the presence of *Z*-methyl cinnamate (Scheme 6). Besides the formation of the expected *E*-ethyl cinnamate, this corollary experiment restituted an 82:18 *Z*/*E* mixture of methyl cinnamate. Visibly, the Pd(0)/AcOH system was responsible for the isomerization of *Z*-cinnamate (see Scheme S3 in the Supporting Information for the mechanistic detail), which is in accordance with the reversibility of the dehydropalladation/reductive elimination sequence.[31]

On the Palladium Reoxidation Step. Coming back to the computational study, the last step of the catalytic cycle is the silver-mediated oxidation of the released $Pd(THF)_2$ (Scheme 7).[32,33] This state is generated after an endergonic product release that reaches 1.2 and 3.2 kcal/mol through a 25.4 and 27.4 kcal/mol rise from the isoenergetic inter-

https://doi.org/10.1021/acs.joc.4c00501
J. Org. Chem. 2024, 89, 10451−10461

Scheme 8. Proposed Mechanism for the Pd-Catalyzed Coupling between Limonene and Methyl Acrylate to Give the Major Product 2*E*,4*E*-3ab

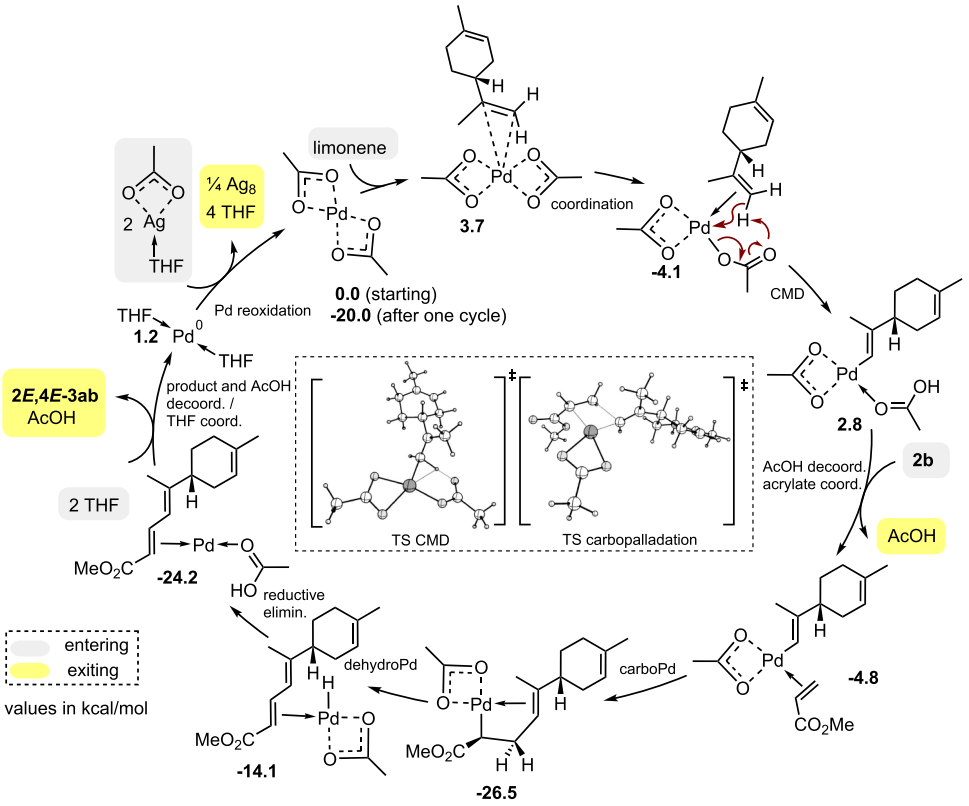

Scheme 9. Observed (Top Right) and Nonobserved (Bottom Right) Pathways after the Carbopalladation Step in the Coupling between Limonene and Allyl Acetate

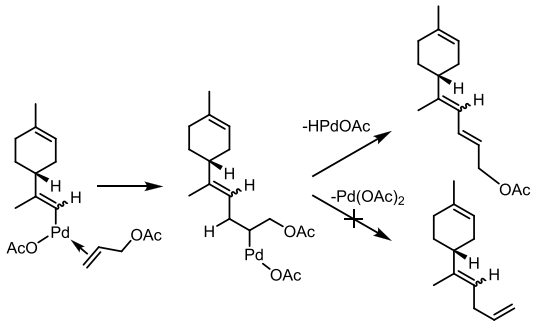

mediates $\mathbf{XI}_{2E4E}$ and $\mathbf{XI}_{2E4Z}$, respectively. In this redox step, Ag(I) is reduced to Ag(0), whose actual state is undetermined. Consideration of the simplest aggregate Ag_2,[34] according to the equation [Pd(0)THF_2 + 2 AgOAc-THF → $Pd(OAc)_2$ + Ag_2 + 4 THF] turns out to be endergonic (Δ_rG° = +2.5 kcal/mol). However, the thermodynamics becomes slightly favorable (Δ_rG° = −11.1 kcal/mol) when the Ag_4 (D_{2h}) aggregate is considered as the silver reduced product, according to the equation [2 Pd(0)-THF_2 + 4 AgOAc-THF → 2 $Pd(OAc)_2$ + Ag_4 + 8 THF], and clearly favorable (Δ_rG° = −84.6 kcal/mol) when the Ag_8 (D_{2h}, dodecahedron)[34d,35] aggregate is considered as the silver reduced product, according to the equation [4 Pd(0)-THF_2 + 8 AgOAc-THF → 4 $Pd(OAc)_2$ + Ag_8 + 16 THF]. Thus, using the latter stoichiometry, the reaction free energy changes (Δ_rG°) of the catalytic cycles relative to the formation of **2*E*,4*E*-3ab** as well as **2*E*,4*Z*-3ab** become −20.0 and −18.0 kcal/mol, respectively. Therefore, assuming that the states relative to $Pd(THF)_2$ are very close in energy and geometry to the corresponding transition states leading to and departing from it, we can predict energetic spans[36] close to 27.7 kcal/mol [+1.2 − (−26.5)] for the 2*E*,4*E* isomer and to 31.1 kcal/mol [(+3.2 − (−27.9)] for the 2*E*,4*Z* isomer. Here again, the computed energy values are

Scheme 10. Sonogashira Coupling under Micellar Catalysis from a C−H/C−H Coupling Product, as Postfunctionalization Example

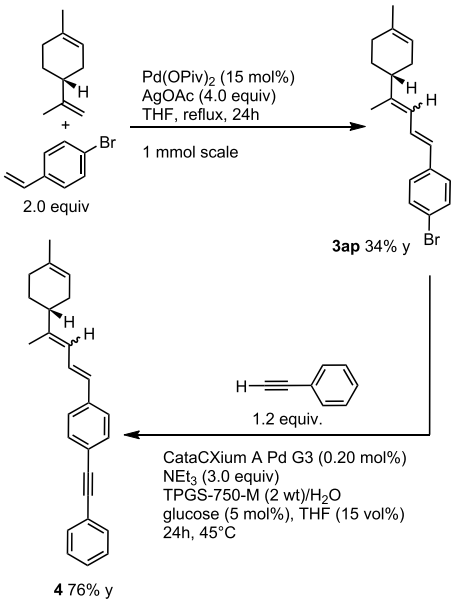

https://doi.org/10.1021/acs.joc.4c00501
J. Org. Chem. 2024, 89, 10451−10461

qualitatively in accord with the observed 2*E*,4*E* (major)/2*E*,4*Z* (minor) isomer ratio of the coupled products and also with the experimental conditions (24 h of THF reflux).

However, the aggregation state of metallic silver is not the only factor affecting the thermodynamics of the palladium reoxidation step. Indeed, the fact that four equivalents of AcOAg are necessary to obtain optimal yields of couplings suggests that on a macroscopic ground, the excess of oxidant[37] has the role of pushing the equilibrium toward the product side, thus securing the regeneration of adequate amounts of $Pd(OAc)_2$. Therefore, while the *E*/*Z* isomeric ratio at the trisubstituted C4=C5 double bond is kinetic in origin, resulting from a different energy span, that at C2=C3 results (for each isomer at C4=C5) from a local thermodynamic control due to product equilibration before its release from the corresponding Pd(0) complex precursor. According to the above DFT computations, the mechanism of the full catalytic cycle relative to the coupling between limonene and methyl acrylate to give the major isomer **2*E*,4*E*-3ab** is proposed in Scheme 8.

Coupling with Allyl Acetate. The mechanism of the coupling between limonene and allyl acetate to give **3an** deserves particular comment.[38] Indeed, the intermediate after the carbopalladation step undergoes dehydropalladation, although deacetoxypalladation could have been an alternative plausible path.[39] We speculate that the allylic nature of the hydrogen atom involved in the dehydropalladation, which in turn generates a conjugated 1,3-diene, is probably the reason for this behavior (Scheme 9).

In view of the nature of our mixed academic/industrial collaborative project, and to further demonstrate the usefulness of this C−H-activation-based, catalytic decoration of limonene, we decided to test a postfunctionalization protocol based on micellar catalysis.[40] This greener type of catalysis may become possible thanks to the presence of surfactants, polymersomes, dendrimers, or nanogels that self-assemble in supramolecular architectures that behave as nanoreactors. In this context, we have recently studied Pd(0) nanoparticles embedded in core−shell nanogels as recoverable catalysts for the Mizoroki−Heck reaction,[41] and we and others have reported a series of articles demonstrating the power of surfactant-promoted, transition-metal-catalyzed chemistry in water at room temperature with possible catalyst recovery.[42] Accordingly, we decided to perform the coupling between limonene and *p*-bromostyrene, and, if successful, to test the resulting product in a Sonogashira coupling[43] using micellar conditions. The planned $C(sp^2)$−H/$C(sp^2)$−H coupling, using the optimized conditions in THF as the solvent, worked as expected, giving bromodiene **3ap** in 34% yield. The Sonogashira coupling was next tackled. After some experimentation (see Supporting Information for the optimization), we found that treatment of **3ao** (1.0 mmol scale) with ethynylbenzene in the presence of the catalytic system [CataCXium-A-Pd-G3 (0.20 mol %), NEt_3 (3.0 equiv), TPGS-750-M (2 wt)/H_2O, glucose (5 mol %)], and THF (15%) as the cosolvent of choice for 24 h at 45 °C gave the desired coupling product **4** in 76% isolated yield (Scheme 10). Notably, these conditions are compared favorably with the classical Sonogashira protocol.[44] The demonstrated sequence allows for a rapid further elaboration of a valorized limonene platform.

CONCLUSIONS

In conclusion, we have developed the first vinyl/vinyl coupling of limonene with several unsaturated partners such as acrylic esters and amides, α,β-unsaturated ketones, styrenes, and allyl acetate. The reaction turned out to be totally regioselective for both reaction partners, involving exclusively the exocyclic unsaturation of limonene without affecting the integrity of the absolute stereochemistry of the C4 stereogenic center of limonene. As to the stereoselectivity, the reaction constantly produced a mixture of the two geometrical isomers 2*E*,4*E* and 2*E*,4*Z*, out of the four possible, with the former always prevailing. On the other hand, the 2*Z* isomers were never detected. In addition, terpenes other than limonene, possessing an isopropenyl function in addition to an endocyclic alkene, such as carvone, perillyl acetate, and valencene, could also be satisfactorily coupled. DFT computation gave results in qualitative accord with the observed selectivity, allowing the proposal of a plausible mechanism for the coupling.

To further valorize the method developed, a large-scale Sonogashira reaction using a C−H/C−H coupled product as a starting substrate was successfully performed under micellar catalysis conditions, allowing its further selective functionalization. Future work will focus on the development of this $C(sp^2)$−H/$C(sp^2)$−H coupling in water, on other selective postfunctionalizations, and on new selective catalytic modifications of terpenes.

ASSOCIATED CONTENT

Data Availability Statement

The data underlying this study are available in the published article, in its Supporting Information, and openly available in Zenodo (10.5281/zenodo.10462156).

Supporting Information

The Supporting Information is available free of charge at https://pubs.acs.org/doi/10.1021/acs.joc.4c00501.

Detailed optimization data, experimental procedures, characterization data, copies of NMR spectra of all new compounds, and DFT computations with coordinates (PDF)

AUTHOR INFORMATION

Corresponding Authors

Alexandre Pradal − *Institut Parisien de Chimie Moléculaire (IPCM), Faculté des Sciences et Ingénierie, CNRS, Sorbonne Université, 75005 Paris, France*; Email: alexandre.pradal@sorbonne-universite.fr

Giovanni Poli − *Institut Parisien de Chimie Moléculaire (IPCM), Faculté des Sciences et Ingénierie, CNRS, Sorbonne Université, 75005 Paris, France*; orcid.org/0000-0002-7356-1568; Email: giovanni.poli@sorbonne-universite.fr

Authors

Marco Di Matteo − *Institut Parisien de Chimie Moléculaire (IPCM), Faculté des Sciences et Ingénierie, CNRS, Sorbonne Université, 75005 Paris, France*

Anna Gagliardi − *Institut Parisien de Chimie Moléculaire (IPCM), Faculté des Sciences et Ingénierie, CNRS, Sorbonne Université, 75005 Paris, France*; Present Address: Institut Lavoisier de Versailles (ILV), Université de Versailles Saint-Quentin-en-Yvelines, Université Paris-Saclay, CNRS, UMR 8180, 45 avenue des États-Unis, 78035 Versailles, France

https://doi.org/10.1021/acs.joc.4c00501
J. Org. Chem. 2024, 89, 10451−10461

Luis F. Veiros − *Centro de Química Estrutural, Institute of Molecular Sciences, Departamento de Engenharia Química, Instituto Superior Técnico, Universidade de Lisboa, 1049 001 Lisboa, Portugal;* orcid.org/0000-0001-5841-3519

Fabrice Gallou − *Novartis Pharma AG, CH-4057 Basel, Switzerland;* orcid.org/0000-0001-8996-6079

Complete contact information is available at: https://pubs.acs.org/10.1021/acs.joc.4c00501

Author Contributions

The manuscript was written through contributions of all authors. All authors have given approval to the final version of the manuscript. For the specific author contributions, see the Supporting Information.

Notes

An earlier version of this manuscript was deposited on a preprint server (10.26434/chemrxiv-2024-nzkq1).[45]
The authors declare no competing financial interest.

■ ACKNOWLEDGMENTS

This work is dedicated to Professor Marta Catellani for her outstanding contribution to palladium chemistry. We warmly thank Dr. Irène Arrata, Project Manager of the European ITN consortium CHAIR https://chair-itn.eu/ for her endless support and encouragement. This project has received funding from the European Union's Horizon 2020 research and innovation program under the Marie Skłodowska-Curie Grant Agreement No 860762. Centro de Química Estrutural (CQE) and Institute of Molecular Sciences (IMS) acknowledge the financial support of Fundação para a Ciência e Tecnologia (Projects UIDB/00100/2020, UIDP/00100/2020, and LA/P/0056/2020, respectively).

■ REFERENCES

(1) SEI, IISD, ODI, E3G, and UNEP, The Production Gap Report 2021, http://productiongap.org/2021report.

(2) Poluzzi, A.; Guandalini, G.; D'Amore, F.; Romano, M. C. The Potential of Power and Biomass-to-X Systems in the Decarbonization Challenge: a Critical Review. *Curr. Sustain. Renew. Energy Rep.* **2021**, *8*, 242−252.

(3) (a) Zhou, C. H.; Xia, X.; Lin, C.-X.; Tong, D.-S.; Beltramini, J. Catalytic Conversion of Lignocellulosic Biomass to Fine Chemicals and Fuels. *Chem. Soc. Rev.* **2011**, *40*, 5588−5617. (b) Chen, G.; Weselake, R. J.; Singer, S. D. (Eds.), *Plant Bioproducts*; Springer New York: New York, NY, 2018.

(4) Dutta, S. Sustainable Synthesis of Drop-In Chemicals from Biomass via Chemical Catalysis: Scopes, Challenges, and the Way Forward. *Energy Fuels* **2023**, *37*, 2648−2666.

(5) Carus, M.; Dammer, L.; Puente, Á.; Raschka, A.; Arendt, O. https://renewable-carbon.eu/publications/product/bio-based-drop-in-smart-drop-in-and-dedicated-chemicals-%E2%88%92-full-version/.

(6) *Bio-Based Chemicals, A 2020 Update, IEA Bioenergy: Task 42: 2020: 01*, https://www.ieabioenergy.com/wp-content/uploads/2020/02/Bio-based-chemicals-a-2020-update-final-200213.pdf.

(7) For review, see: (a) Dalton, T.; Faber, T.; Glorius, F. C−H Activation: Toward Sustainability and Applications. *ACS Cent. Sci.* **2021**, *7*, 245−261. (b) Rogge, T.; Kaplaneris, N.; Chatani, N.; Kim, J.; Chang, S.; Punji, B.; Schafer, L. L.; Musaev, D. G.; Wencel-Delord, J.; Roberts, C. A.; Sarpong, R.; Wilson, Z. E.; Brimble, M. A.; Johansson, M. J.; Ackermann, L. C−H activation. *Nat. Rev. Methods Primer* **2021**, *43*, 1−31. (c) Roudesly, F.; Oble, J.; Poli, G. Metal-catalyzed C−H Activation/functionalization: The Fundamentals. *J. Mol. Catal. Chem. A* **2017**, *426*, 275−296. (d) de Jesus, R.; Hiesinger, K.; van Gemmeren, M. Preparative Scale Applications of C−H Activation in Medicinal Chemistry. *Angew. Chem., Int. Ed.* **2023**, *62*, No. e202306659.

(8) (a) Breitmaier, E.. *Terpenes: Flavors, Fragrances, Pharmaca, Pheromones*, Ed.: Breitmaier, E.; Wiley-VCH: Weinheim, 2006. (b) Brill, Z. G.; Condakes, M. L.; Ting, C. P.; Maimone, T. J. Navigating the Chiral Pool in the Total Synthesis of Complex Terpene Natural Products. *Chem. Rev.* **2017**, *117*, 11753−11795. (c) Winnacker, M. Polyamides Derived from Terpenes: Advances in Their Synthesis, Characterization and Applications. *Eur. J. Lipid Sci. Technol.* **2023**, *125*, No. 2300014.

(9) For reviews on $C(sp^2)$−H/$C(sp^2)$−H coupling involving plain alkenes, see: (a) Shang, X.; Liu, Z.-Q. Transition Metal-catalyzed Cvinyl−Cvinyl Bond Formation via Double Cvinyl−H Bond Activation. *Chem. Soc. Rev.* **2013**, *42*, 3253−3260. (b) Maikhuri, V. K.; Maity, J.; Srivastavac, S.; Prasad, A. K. Transition metal-catalyzed double Cvinyl−H bond activation: synthesis of conjugated dienes. *Org. Biomol. Chem.* **2022**, *20*, 9522−9588.

(10) For precedents of Pd-catalyzed nondirected $C(sp^2)$−H/$C(sp^2)$−H couplings involving plain alkenes, see: (a) da Silva, M. J.; Gusevskaya, E. V. Palladium-catalyzed oxidation of monoterpenes: novel tandem oxidative coupling−oxidation of camphene by dioxygen. *J. Mol. Catal. A: Chem.* **2001**, *176*, 23−27. (b) da Silva, M. J.; Gonçalves, J. A.; Alves, R. B.; Howarth, O. W.; Gusevskaya, E. V. Palladium Catalyzed Transformations of Monoterpenes: Stereoselective Deuteriation and Oxidative Dimerization of Camphene. *J. Organomet. Chem.* **2004**, *689*, 302−308. (c) Hatamoto, Y.; Sakaguchi, S.; Ishii, Y. Oxidative Cross-Coupling of Acrylates with Vinyl Carboxylates Catalyzed by a $Pd(OAc)_2$/HPMoV/O_2 System. *Org. Lett.* **2004**, *6*, 4623−4625. (d) Xu, Y. H.; Lu, J.; Loh, T.-P. Direct Cross-Coupling Reaction of Simple Alkenes with Acrylates Catalyzed by Palladium Catalyst. *J. Am. Chem. Soc.* **2009**, *131*, 1372−1373. (e) Xu, Y.-H.; Wang, W.-J.; Wen, Z.-K.; Hartley, J. J.; Loh, T.-P. Palladium-Catalyzed Direct Cross-coupling Reaction between Indenes and Electron-deficient Alkenes. *Tetrahedron Lett.* **2010**, *51*, 3504−3507. (f) Yu, H.; Jin, W.; Sun, C.; Chen, J.; Du, W.; He, S.; Yu, Z. Palladium-Catalyzed Cross-Coupling of Internal Alkenes with Terminal Alkenes to Functionalized 1,3-Butadienes Using C−H Bond Activation: Efficient Synthesis of Bicyclic Pyridones. *Angew. Chem., Int. Ed.* **2010**, *49*, 5792−5797. (g) Wen, Z.-K.; Xu, Y.-H.; Loh, T.-P. Palladium(II)-catalyzed Cross-coupling of Simple Alkenes with Acrylates: a Direct Approach to 1,3-Dienes through C−H Activation. *Chem. Sci.* **2013**, *4*, 4520−4524. (h) Wen, Z. K.; Xu, Y. H.; Loh, T.-P. Palladium-Catalyzed Cross-Coupling of Unactivated Alkenes with Acrylates: Application to the Synthesis of the C13−C21 Fragment of Palmerolide A. *Chem.—Eur. J.* **2012**, *18*, 13284−13287. (i) Zhang, X.; Wang, M.; Zhang, M.-X.; Xu, Y.-H.; Loh, T.-P. Synthesis of Dienyl Ketones via Palladium(II)-Catalyzed Direct Cross-Coupling Reactions between Simple Alkenes and Vinyl Ketones: Application to the Synthesis of Vitamin A1 and Bornelone. *Org. Lett.* **2013**, *15*, 5531−5533.

(11) For precedents of Pd-catalyzed nondirected $C(sp^2)$−H/$C(sp^2)$−H couplings involving heteroatom-enriched alkenes, see: (a) Gigant, N.; Bäckvall, J.-E. Synthesis of Conjugated Dienes via a Biomimetic Aerobic Oxidative Coupling of Two Cvinyl−H Bonds. *Chem.—Eur. J.* **2013**, *19*, 10799−10803. (b) Gigant, N.; Gillaizeau, I. Palladium(II)-Catalyzed Direct Alkenylation of Nonaromatic Enamides. *Org. Lett.* **2012**, *14*, 3304−3307. (c) Chen, Y.; Wang, F.; Jia, A.; Li, X. Palladium-Catalyzed Selective Oxidative Olefination and Arylation of 2-Pyridones. *Chem. Sci.* **2012**, *3*, 3231−3236. (d) Yu, Y.-Y.; Georg, G. I. Dehydrogenative Alkenylation of Uracils via Palladium-catalyzed Regioselective C−H Activation. *Chem. Commun.* **2013**, *49*, 3694−3696. (e) Yu, Y.-Y.; Niphakis, M. J.; Georg, G. I. Palladium(II)-Catalyzed Dehydrogenative Alkenylation of Cyclic Enaminones via the Fujiwara−Moritani Reaction. *Org. Lett.* **2011**, *13*, 5932−5935. (f) Ge, H.; Niphakis, M. J.; Georg, G. I. Palladium(II)-Catalyzed Direct Arylation of Enaminones Using Organotrifluoroborates. *J. Am. Chem. Soc.* **2008**, *130*, 3708−3709. (g) Li, M.; Li, L.; Ge, H. Direct C-3-Alkenylation of Quinolones via Palladium-Catalyzed C−H Functionalization. *Adv. Synth. Catal.* **2010**,

352, 2445−2449. (h) Kim, D.; Hong, S. Palladium(II)-Catalyzed Direct Intermolecular Alkenylation of Chromones. *Org. Lett.* **2011**, *13*, 4466−4469. (i) Min, M.; Kim, Y.; Hong, S. Regioselective Palladium-catalyzed Olefination of Coumarins via Aerobic Oxidative Heck Reactions. *Chem. Commun.* **2013**, *49*, 196−198. (j) Moon, Y.; Kwon, D.; Hong, S. Palladium-Catalyzed Dehydrogenation/Oxidative Cross-Coupling Sequence of β-Heteroatom-Substituted Ketones. *Angew. Chem., Int. Ed.* **2012**, *51*, 11333−11336.

(12) For precedents of Pd-catalyzed directed C(sp^2)−H/C(sp^2)−H couplings, see: (a) Xu, Y.-H.; Chok, Y.-K.; Loh, T.-P. Synthesis and Characterization of a Cyclic Vinylpalladium(II) Complex: Vinylpalladium Species as the Possible Intermediate in the Catalytic Direct Olefination Reaction of Enamide. *Chem. Sci.* **2011**, *2*, 1822−1825. (b) Zhao, Q.; Tognetti, V.; Joubert, L.; Besset, T.; Pannecoucke, X.; Bouillon, J.-P.; Poisson, T. Palladium-Catalyzed Synthesis of 3-Trifluoromethyl-Substituted 1,3-Butadienes by Means of Directed C−H Bond Functionalization. *Org. Lett.* **2017**, *19*, 2106−2109. (c) Liu, M.; Yang, P.; Karunananda, M. K.; Wang, Y.; Liu, P.; Engle, K. M. C(alkenyl)−H Activation via Six-Membered Palladacycles: Catalytic 1,3-Diene Synthesis. *J. Am. Chem. Soc.* **2018**, *140*, 5805−5813. (d) Schreib, B. S.; Son, M.; Aouane, F. A.; Baik, M.-H.; Carreira, E. M. Allene C(sp^2)−H Activation and Alkenylation Catalyzed by Palladium. *J. Am. Chem. Soc.* **2021**, *143*, 21705−21712. (e) Liang, Q.-J.; Yang, C.; Meng, F.-F.; Jiang, B.; Xu, Y.-H.; Loh, T.-P. Chelation versus Non-Chelation Control in the Stereoselective Alkenyl sp^2 C−H Bond Functionalization Reaction. *Angew. Chem., Int. Ed.* **2017**, *56*, 5091−5095. (f) Meng, K.; Li, T.; Yu, C.; Shen, C.; Zhang, J.; Zhong, G. Geminal Group-Directed Olefinic C−H Functionalization via Four- to Eight-membered Exo-metallocycles. *Nat. Commun.* **2019**, *10*, 5109. (g) Liu, M.; Sun, J.; Erbay, T. G.; Ni, H.-Q.; Martín-Montero, R.; Liu, P.; Engle, K. M. Pd(II)-Catalyzed C(alkenyl)−H Activation Facilitated by a Transient Directing Group. *Angew. Chem., Int. Ed.* **2022**, *61*, No. e202203624.

(13) For other Rh- or Ru-catalyzed directed C(sp^2)−H/C(sp^2)−H couplings, see: (a) Besset, T.; Kuhl, N.; Patureau, F. W.; Glorius, F. Rh(III)-Catalyzed Oxidative Olefination of Vinylic C−H Bonds: Efficient and Selective Access to Di-unsaturated α-Amino Acid Derivatives and Other Linear 1,3-Butadienes. *Chem.—Eur. J.* **2011**, *17*, 7167−7171. (b) Boultadakis-Arapinis, M.; Hopkinson, M. N.; Glorius, F. Using Rh(III)-Catalyzed C−H Activation as a Tool for the Selective Functionalization of Ketone-Containing Molecules. *Org. Lett.* **2014**, *16*, 1630−1633. (c) Hu, X.-H.; Zhang, J.; Yang, X.-F.; Xu, Y.-H.; Loh, T.-P. Stereo- and Chemoselective Cross-Coupling between Two Electron-Deficient Acrylates: An Efficient Route to (Z,E)-Muconate Derivatives. *J. Am. Chem. Soc.* **2015**, *137*, 3169−3172. (d) Feng, R.; Yu, W.; Wang, K.; Liu, Z.; Zhang, Y. Ester-Directed Selective Olefination of Acrylates by Rhodium Catalysis. *Adv. Synth. Catal.* **2014**, *356*, 1501−1508. (e) Li, F.; Yu, C.; Zhang, J.; Zhong, G. Weinreb Amide Directed Cross-coupling Reaction between Electron-deficient Alkenes Catalyzed by a Rhodium Catalyst. *Org. Biomol. Chem.* **2017**, *15*, 1236−1244. (f) Logeswaran, R.; Jeganmohan, M. Rhodium(III)-Catalyzed Aerobic Oxidative C−H Olefination of Unsaturated Acrylamides with Unactivated Olefins. *Org. Lett.* **2021**, *23*, 767−771. (g) Zhanga, J.; Loh, T.-P. Ruthenium- and Rhodium-catalyzed Cross-coupling Reaction of Acrylamides with Alkenes: Efficient Access to (Z,E)-Dienamides. *Chem. Commun.* **2012**, *48*, 11232−11234. (h) Hu, X.-H.; Yang, X.-F.; Loh, T.-P. Selective Alkenylation and Hydroalkenylation of Enol Phosphates through Direct C−H Functionalization. *Angew. Chem., Int. Ed.* **2015**, *54*, 15535−15539.

(14) Watson, D. A.; Reid, W. B. Synthesis of Trisubstituted Alkenyl Boronic Esters from Alkenes Using the Boryl-Heck Reaction. *Org. Lett.* **2018**, *20*, 6832−6835.

(15) Kollár, L.; Bakos, J.; Heil, B.; Sándor, P.; Szalontai, G. J. Hydroformylation of Chiral Terpenes with $PtCl(SnCl_3)$-(bis-phosphine) as Catalyst. *Organomet. Chem.* **1990**, *385*, 147−152.

(16) Vieira, C. G.; de Freitas, M. C.; dos Santos, E. N.; Gusevskaya, E. V. Synthesis of Fragrance Ingredients by Tandem Hydroformylation-Cyclization of Limonene Catalyzed by Rhodium Complexes and Pyridinium p-Toluenesulphonate. *ChemCatChem.* **2012**, *4*, 795−801.

(17) Causero, A.; Troll, C.; Rieger, B. (+)-Limonene Functionalization: Syntheses, Optimization, and Scale-up Procedures for Sustainable Polymer Building Blocks. *Ind. Eng. Chem. Res.* **2020**, *59*, 15464−15477.

(18) The complex *n*-BuLi/TMEDA is known to metalate limonene at C-10: Crawford, R. J.; Erman, W. F.; Broaddus, C. D. Metalation of Limonene. A Novel Method for the Synthesis of Bisabolane Sesquiterpenes. *J. Am. Chem. Soc.* **1972**, *94*, 4298−4306.

(19) Acrylic acid, and thus acrylates, can also be biobased, resulting from the dehydration of lactic acid or 3-hydroxypropionic acid, or from dehydration/oxidation of glycerol. See: Brobbey, M. S.; Louw, J.; Görgens, J. F. Biobased Acrylic Acid Production in a Sugarcane Biorefinery: A Techno-economic Assessment Using Lactic Acid, 3-Hydroxypropionic Acid and Glycerol as Intermediates. *Chem. Eng. Res. Des.* **2023**, *193*, 367−382.

(20) (a) Carole, W. A.; Colacot, T. J. Understanding Palladium Acetate from a User Perspective. *Chem.—Eur. J.* **2016**, *22*, 7686−7695. (b) Carole, W. A.; Colacot, T. J. Unravelling the Mystery of Palladium Acetate. Investigations of high purity palladium acetate and its two common impurities. *Chim. Oggi-Chem. Today* **2017**, *35*, 64−65.

(21) For other oxidizing agents tested, see the Supporting Information.

(22) Other terminal oxidants were also considered for this coupling ($Cu(OAc)_2$, $CuCl_2$, $AgCO_3$, Ag_2O, DMBQ, PIDA, BQ, Oxone®, H_2O_2, t-BuO_2H, $AgNO_3$ and $K_2S_2O_8$). However, none of these oxidants performed better than AgOAc.

(23) Experiments of the model coupling reaction using 2-MeTHF, dimethyl isosorbide, or Cyrene® as solvent gave unsatisfactory yields (see Supporting Information).

(24) Preparation of compound **3ab** was also performed on a 16.2 mmol scale providing the desired product with 47% isolated yield and a d.r. of 69:31.

(25) The low yield of **3af** and **3ag** was due to difficulties to separate the product from the starting acrylate during purification.

(26) We only considered tertiary acrylamides, as primary and secondary acrylamides are expected to be incompatible with this coupling.

(27) The low yield of this product is mainly due its high volatility.

(28) Other electron-poor alkene partners such as acrylonitrile, phenylvinylsulfoxide, vinyl diethylphosphonate or 5,6-dihydro-2*H*-pyran-2-one did not provide the desired coupling product. No conversion was observed with acrylonitrile and phenylvinylsulfoxide. Full conversion but very low yields (<5%) were obtained with vinyl diethylphosphonate or 5,6-dihydro-2*H*-pyran-2-one.

(29) (a) Parr, R. G.; Yang, W. *Density Functional Theory of Atoms and Molecules*; Oxford University Press: New York, 1989. (b) Calculations performed at the PBE0-D3/(SDD*,6-311++G(d,p)//PBE0/(SDD*,6-31G(d,p)) level using the GAUSSIAN 09 package. Solvent effects (THF) were considered using the PCM/SMD model. A full account of the computational details and a complete list of references are provided as Supporting Information.

(30) Before performing the DFT studies, three mechanistic hypotheses relative to the first palladation event were initially considered (see Scheme S2).

(31) Sommer, H.; Juliá-Hernández, F.; Martin, R.; Marek, I. Walking Metals for Remote Functionalization. *ACS Cent. Sci.* **2018**, *4*, 153−165.

(32) Some studies on Pd-catalysis in the presence of silver salts invoke the intervention of bimetallic Pd/Ag species (see next reference). However, a coupling reaction carried out between limonene and ethyl acrylate using a stoichiometric amount of $Pd(OAc)_2$ and in the absence of AgOAc, gave the expected product **3aa** in 50% isolated yield (71:29 E/Z). This result suggests that the silver salt in this coupling is only responsible for the Pd(0) reoxidation step.

https://doi.org/10.1021/acs.joc.4c00501
J. Org. Chem. 2024, 89, 10451−10461

(33) (a) de Carvalho, R. L.; Diogo, E. B. T.; Homölle, S. L.; Dana, S.; da Silva, E. N., Jr; Ackermann, L. The Crucial Role of Silver(I)-salts as Additives in C−H Activation Reactions: Overall Analysis of Their Versatility and Applicability. *Chem. Soc. Rev.* **2023**, *52*, 6359−6378. (b) Pérez-Ortega, I.; Albéniz, A. C. Multifaceted Role of Silver Salts as Ligand Scavengers and Different Behavior of Nickel and Palladium complexes: Beyond Halide Abstraction. *Dalton Trans.* **2023**, *52*, 1425−1432. (c) Bhattacharya, T.; Dutta, S.; Maiti, D. Deciphering the Role of Silver in Palladium-Catalyzed C−H Functionalizations. *ACS Catal.* **2021**, *11*, 9702−9714. (d) Malakar, S.; Schaefer, H. F.; Sunoj, R. B. Is Silver a Mere Terminal Oxidant in Palladium Catalyzed C−H Bond Activation Reactions? *Chem. Sci.* **2020**, *11*, 208−216. (e) Bay, K. L.; Yang, Y.-F.; Houk, K. N. Multiple Roles of Silver Salts in Palladium-catalyzed C−H Activations. *J. Organomet. Chem.* **2018**, *864*, 19−25. (f) Funes-Ardoiz, I.; Maseras, F. Oxidative Coupling Mechanisms: Current State of Understanding. *ACS Catal.* **2018**, *8*, 1161−1172. (g) Anand, M.; Sunoj, R. B.; Shaefer, H. F., III Non-innocent Additives in a Palladium(II)-Catalyzed C−H Bond Activation Reaction: Insights into Multimetallic Active Catalysts. *J. Am. Chem. Soc.* **2014**, *136*, 5535−5538. (h) Yang, Y.-F.; Cheng, G.-J.; Liu, P.; Leow, D.; Sun, T.-Y.; Chen, P.; Zhang, X.; Yu, J.-Q.; Wu, Y.-D.; Houk, K. N. Palladium-Catalyzed Meta-Selective C−H Bond Activation with a Nitrile-Containing Template: Computational Study on Mechanism and Origins of Selectivity. *J. Am. Chem. Soc.* **2014**, *136*, 344−355.

(34) (a) Pereiro, M.; Baldomir, D.; Arias, J. E. Unexpected Magnetism of Small Silver Clusters. *Phys. Rev. A* **2007**, *75*, No. 063204. (b) Pereiro, M.; Baldomir, D. Structure of Small Silver Clusters and Static Response to an External Electric Field. *Phys. Rev. A* **2007**, *75*, No. 033202. (c) Pereiro, M.; Baldomir, D. Determination of the Lowest-energy Structure of Ag_8 from First-principles Calculations. *Phys. Rev. A* **2005**, *72*, No. 045201. (d) Tsuneda, T. Theoretical Investigations on Geometrical and Electronic Structures of Silver Clusters. *J. Comput. Chem.* **2019**, *40*, 206−211.

(35) Ag octamers (n = 8), and octakaidecamers (n = 18) are considered to become more stable than other clusters.

(36) In truth, the energetic span is the difference between the energy of the transition state leading to $Pd(THF)_2$, which is expected to be the turnover frequency determining transition state (TDTS) and that of the resting state. However, as the step of the release of $Pd(THF)_2$ is highly endergonic, according to the Hammond postulate, it should feature a rather late transition state, energetically and geometrically very similar to the state of $Pd(THF)_2$.

(37) (a) Solel, E.; Tarannam, N.; Kozuch, S. Catalysis: Energy is the Measure of All Things. *Chem. Commun.* **2019**, *55*, 5306−5322. (b) Besora, M.; Maseras, F. Microkinetic Modeling in Homogeneous Catalysis. *WIREs Comput. Mol. Sci.* **2018**, *8*, No. e1372.

(38) Zhang, Y.; Cui, Z.; Li, Z. J.; Liu, Z.-Q. Pd(II)-Catalyzed Dehydrogenative Olefination of Vinylic C−H Bonds with Allylic Esters: General and Selective Access to Linear 1,3-Butadienes. *Org. Lett.* **2012**, *14*, 1838−1841. For a similar type of coupling, see:

(39) (a) Zhao, H.; Ariafard, A.; Lin, Z. β-Heteroatom versus β-Hydrogen Elimination: A Theoretical Study. *Organometallics* **2006**, *25*, 812−819. (b) Bogdos, M. K.; Stepanović, O.; Bismuto, A.; Luraschi, M. G.; Morandi, B. Mechanistically Informed Selection Rules for Competing β-Hydride and β-Heteroatom Eliminations. *Nat. Chem.* **2022**, *1*, 787−793. (c) Ferber, B.; Prestat, G.; Vogel, S.; Madec, D.; Poli, G. Synthesis of 3,5-Disubstituted Piperazinones via Palladium (II) -Catalyzed Amination. *Synlett* **2006**, *13*, 2133−2135.

(40) (a) Fabris, F.; Illner, M.; Repke, J.-U.; Scarso, A.; Schwarze, M. Is Micellar Catalysis Green Chemistry? *Molecules* **2023**, *28*, 4809. (b) Roschangar, F.; Zhou, Y.; Constable, D. J. C.; Colberg, J.; Dickson, D. P.; Dunn, P. J.; Eastgate, M. D.; Gallou, G.; Hayler, J. D.; Koenig, S. G.; Kopach, M. E.; Leahy, D. K.; Mergelsberg, I.; Scholz, U.; Smith, A. G.; Henry, M.; Mulder, J.; Brandenburg, J.; Dehli, J. R.; Fandrick, D. R.; Fandrick, K. R.; Gnad-Badouin, F.; Zerban, G.; Groll, K.; Anastas, P. T.; Sheldon, R. A.; Senanayake, C. H. Inspiring Process Innovation via an Improved Green Manufacturing Metric: iGAL. *Green Chem.* **2018**, *20*, 2206−2211.

(41) Pontes da Costa, A.; Nunes, D. R.; Tharaud, M.; Oble, J.; Poli, G.; Rieger, J. Palladium(0) Nanoparticles Embedded in Core−shell Nanogels as Recoverable Catalysts for the Mizoroki−Heck Reaction. *ChemCatChem.* **2017**, *9*, 2167−2175.

(42) For some recent reviews, see: (a) De Martino, M. T.; Abdelmohsen, L. K. E. A.; Rutjes, F. P. J. T.; van Hest, J. C. M. Nanoreactors for Green Catalysis. *Beilstein J. Org. Chem.* **2018**, *14*, 716−733. (b) Lipshutz, B. H.; Ghorai, S.; Cortes-Clerget, M. The Hydrophobic Effect Applied to Organic Synthesis: Recent Synthetic Chemistry "in Water. *Chem.—Eur. J.* **2018**, *24*, 6672−6695. (c) Cortes-Clerget, M.; Yu, J.; Kincaid, J. R. A.; Walde, P.; Gallou, F.; Lipshutz, B. H. Water as the Reaction Medium in Organic Chemistry: from our Worst Enemy to our Best Friend. *Chem. Sci.* **2021**, *12*, 4237−4266.

(43) For precedents of Sonogashira couplings under micellar conditions, see: (a) Lipshutz, B. H.; Chung, D. W.; Rich, B. Sonogashira Couplings of Aryl Bromides: Room Temperature, Water Only. *No Copper. Org. Lett.* **2008**, *10*, 3793−3796. (b) Jakobi, M.; Gallou, F.; Sparr, C.; Parmentier, M. A General Protocol for Robust Sonogashira Reactions in Micellar Medium. *Helv. Chim. Acta* **2019**, *102*, No. e1900024. (c) Braje, W.; Britze, K.; Dietrich, J. D.; Jolit, A.; Kaschel, J.; Klee, J.; Lindner, T. Organic Reactions Carried out in Aqueous Solution in the Presence of a Hydroxyalkyl(alkyl)cellulose or an Alkylcellulose. Patent 2017, WO 2017/129796. (d) Struwe, J.; Ackermann, L.; Gallou, F. Recent Progress in Copper-free Sonogashira-Hagihara Cross-couplings in Water. *Chem. Catal* **2023**, *3*, No. 100485.

(44) The same coupling carried out under classical conditions on a 1.0 mmol scale with the catalytic system [$PdCl_2(PPh_3)_2$ (0.2 mol%), CuI (5 mol%), NEt_3 (3.0 equiv.)] in DMF for 24 h at 45 °C, afforded **4** in 44% isolated yield.

(45) Poli, G.; Pradal, A.; Di Matteo, M.; Gagliardi, A.; Veiros, L.; Gallou, F. First Pd-catalyzed C(sp2)−H / C(sp2)−H coupling of Limonene. *ChemRxiv* **2024**, DOI: 10.26434/chemrxiv-2024-nzkq1.

https://doi.org/10.1021/acs.joc.4c00501
J. Org. Chem. 2024, 89, 10451−10461